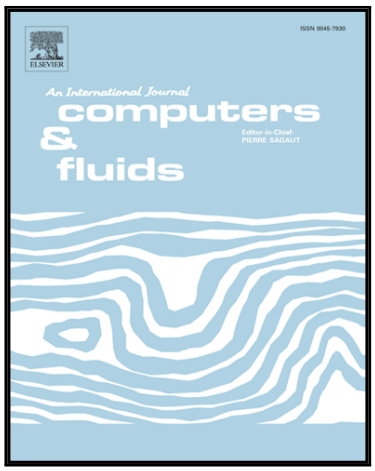

A new implementation method of sharp interface boundary conditions for particle methods in simulating wave interaction with submerged porous structure

Yan Zhou , Ping Dong

PII: S0045-7930(18)30692-3
DOI: https://doi.org/10.1016/j.compfluid.2018.09.022
Reference: CAF 4020

To appear in: *Computers and Fluids*

Received date: 12 June 2018
Revised date: 28 August 2018
Accepted date: 27 September 2018

Please cite this article as: Yan Zhou , Ping Dong , A new implementation method of sharp interface boundary conditions for particle methods in simulating wave interaction with submerged porous structure, *Computers and Fluids* (2018), doi: https://doi.org/10.1016/j.compfluid.2018.09.022

Highlights

- New implementation method of interface conditions for flow over porous media
- Single layer of interface particle without smoothing of any parameters.
- Validated by analytical solutions and experimental data for solitary waves
- Validated by propagating waves with wave breaking on the structure.

A new implementation method of sharp interface boundary conditions for particle methods in simulating wave interaction with submerged porous structure

Yan Zhou[1*], Ping Dong[1]

[1] School of Engineering, University of Liverpool, Liverpool, UK
* Corresponding author

Abstract

A new formulation of interface boundary conditions for simulating water waves over submerged porous media using particle method is presented. The fluid flow over and through a porous media is modelled by the standard NS equations for the free flow and volume averaged NS equation based on the Forcheimmer's type resistant force for the flow in the porous media, respectively. As the porosity and resistant forces exist only within the porous media, the continuity of Darcy velocity and flow stresses need to be enforced at the interface boundary between the free flow and the flow in the porous media. These boundary conditions are implemented simultaneously at the stage of solving the Poisson pressure equation (PPE) by transforming the velocity condition to an expression of pressure gradient and then applying the pressure expression at the sharp interface incorporating the stress conditions. Implementing the new formulation within the framework of an existing particle-based code (MLPG_R), a set of numerical 'experiments' is performed to demonstrate the method's effectiveness as compared with analytical solutions and experimental data including solitary wave and regular propagating wave with wave breaking.

Key words: porous media, interface treatment, particle method, coastal breakwater

1. Introduction

Man-made structures such as submerged breakwaters or revetments built of porous materials are widely used to protect natural coastline or coastal infrastructures from erosion or flooding damages. The porous materials exert skeleton resistant forces on the flow and thus can result in flow energy dissipation. The accurate prediction of the flow processes within and around the porous structure is therefore crucial in predicting the wave transmission, reflection and damping as well as assessing the functional performance and stability of the porous structures. In the past two decades, a range of numerical models for investigations of flow over porous structures have been developed based on linear wave theory [1, 2], nonlinear shallow water equations (e.g. [3]) and more recently full Navier-Stokes (NS) equations [4, 5] which are capable of dealing with complex flow processes such as wave breaking and removing many of the simplifying assumptions in potential flow models.

For solving the NS equations, there are two standard approaches: microscopic and macroscopic approaches. The microscopic approach resolves flow interaction with each solid element in the porous media and the flow resolution is at the pore scale. Due to the high demand on computational resources to achieve such detailed solution this approach is generally taken when considering small scale domains such as pore-scale multiphase simulation in oil and gas industry [6]. On the other hand, the macroscopic approach considers only volume-averaged flow behaviour without resolving the real pore geometries. The mean flow in porous media is governed by volume-averaged NS equations in which linear and nonlinear resistant terms are added to represent laminar and turbulence-induced frictional forces, respectively [2]. These two terms may adopt different types of parameterisations [7, 8] experimentally tested for various solid-phase types and flow regimes. In coastal engineering the main interest is usually on the large scale behaviour of the flow when moving over or through the porous structures rather than on the flow details within the pores, which makes the second approach more attractive.

Once the porous flow equations are determined, the matching conditions (or coupling schemes) at the interface of the free flow and flow in the porous structure are required to complete the model. For both mesh-based or particle-based methods, two main types of interface treatments can be found in the literatures, one is to adopt an unified flow equation by smearing porous properties and corresponding resistant terms across the interface [9-11] and the other is to enforce stress and velocity conditions explicitly at the interface boundary [5,12]. In the unified equation approach the resistant force is transferred smoothly over a small transitional region from a physical value within the porous media to zero outside the media and the interface conditions are thus inherently satisfied. This method has been incorporated into mesh-based method by solving an extra transport equation for determining porosity weighting in the transitional region [13,14]. When the concept was introduced to particle-based SPH method, the porosity carried by transitional particle is interpolated from a set of background particles [9] with all variables updated by one set of equations. Ren et al. [15] improved this scheme by reducing the thickness of the transitional layer to solve pressure but updating velocity by equations based on unsmoothed porosities. A compensation for velocity continuity was introduced in Ren et al. [10] by smoothing out the velocity for particles within the transition layer. Based also on the unified equations similar smoothing technique was applied by Gui et al. [16] to the pressure as an alternative interface condition. To ensure the stability and accuracy of predicted flows in the transitional layer this unified equation approach requires extra efforts on porosity smoothing and transitional thickness control. In the second approach, the interface conditions are enforced explicitly at mesh edges or a layer of particles that are generated to match the geometry of the porous structure. In mesh-based method, pressure and velocity conditions are iteratively matched within each time step which is computationally expensive [12] while for particle-based method in this group, Shao [5] matched pressure and velocity on the interface particles by obtaining boundary values for porous domain from the free flow domain through SPH interpolation scheme and vice versa. Other approximate interface treatments are also proposed such as modified log-wall function method by [4] that incorporates characteristics of the porous media to represent the turbulent flow near the porous bed [17] and surface integrals over the interface to obtain interfacial momentum transfer in which interface conditions are not incorporated [18].

In this work, a method is developed and tested that implements the interface conditions on a single layer of particles representing a sharp boundary of the porous media domain thus removing the need for transitional interfaces zones and associated artificial treatments. An explicit pressure expression is derived as a Dirichlet condition for solving pressure Poisson's equations for both domains. By converting the interface conditions of stress and Darcy velocity continuities to that relate to pressure and pressure gradient terms between two domains, the pressure for the interface particle is derived based on Taylor expansion of pressure near the interface with two interface conditions implemented. The implementation procedure is similar to that in the two-phase flow model of Zhou [19] but is further developed to deal with Darcy velocity continuity which results in a situation that the intrinsic velocities are not continuous at the interface but with a ratio of the porosity. Such implementation scheme is applied for the first time to simulate flow over porous media. As the porous media is rigid, interface particles are fixed in space on which the boundary conditions coupling the two domains are applied while particles within each domain are allowed to move freely in a Lagrangian manner taking on the local properties when they move across the interface. This treatment is similar to that for slip rigid boundary conditions in particle-based method [20] in which the pressure and velocity are updated for wall particles while the positions are fixed.

The paper is organised as follows: after the Introduction, the governing equations for flows inside and outside the porous media are provided in Section 2 followed by interface and boundary conditions. Numerical schemes including solving two sets of equations separately, the numerical implementation procedures of the interface conditions and treatments of particles on rigid wall, free surface and wave absorption zone are presented in Section 3. Model validations are carried out in Section 4 against both analytical solutions and experimental data including solitary and propagating waves and porous media

in the types of porous bed, rectangular and trapezoid breakwaters. Finally a conclusion is drawn in Section 5.

2. Governing equations

The simulated fluid domain is spilt into two regions which are inside and outside the porous media, respectively. The pure fluid flow outside the porous media is governed by the usual NS equations while the flow inside the porous media is governed by the volume averaged NS equation containing additional source terms to account for the effects of solid skeleton on the flow. The continuity of flow and stresses across the boundary between the two regions is enforced by implementing the proposed interface conditions to be discussed in Section 3.2.

2.1 Equations for flow outside porous media

The standard incompressible Navier-Stokes equations are applied for the flow. The continuity equation can be written as

$$\nabla \cdot \boldsymbol{u}_l = 0 \tag{1}$$

where $\boldsymbol{u}_l$ is the velocity of the fluid outside the porous media. In some previous models based on particle methods, turbulence has been considered by adding the Sub-Particle- Scale (SPS) turbulence stress [10,21] in the momentum equations, which is equivalent to sub-grid-scale stress in mesh based methods. However, as indicated in [10], wave surface elevation around porous coastal structures calculated with or without the turbulence effects differ only slightly, even near the breaking point. Thus, to demonstrate the effectiveness of the new interface treatment method with an efficient model, the flow is treated in this work as laminar and the momentum equation in Lagrangian form is

$$\frac{d\boldsymbol{u}_l}{dt} = -\frac{1}{\rho}\nabla p_l + \boldsymbol{g} + \nu\nabla^2\boldsymbol{u}_l \tag{2}$$

where p_l is the pressure of the fluid outside the porous structure, ν is the kinematic viscosity of the fluid and $\boldsymbol{g}$ is gravitational acceleration.

2.2 Equations for flow inside porous media

Within the porous media, the flow is governed by the spatial averaged Navier-Stokes type equations based on the classical Forcheimmer's type resistant force formulation, which read as

$$\nabla \cdot \boldsymbol{u}_p = 0 \tag{3}$$

$$(1+S)\frac{d\boldsymbol{u}_p}{dt} = -\frac{1}{\rho}\nabla p_p + \boldsymbol{g} + \nu\nabla^2\boldsymbol{u}_p - \frac{\nu n_w}{K_p}\boldsymbol{u}_p - \frac{C_f {n_w}^2}{\sqrt{K_p}}\boldsymbol{u}_p|\boldsymbol{u}_p| \tag{4}$$

where n_w is porosity, $\boldsymbol{u}_p$ is the seepage velocity which can be converted to the Darcy velocity $\boldsymbol{u}_D$ by $\boldsymbol{u}_D = \boldsymbol{u}_p n_w$, p_p is the fluid pressure within the porous media. The last two terms in Eq. (4), one linear and one nonlinear, represent the resistance exerted on the fluid by the solid skeleton of the porous media. K_p (m^2) is intrinsic permeability and according to Furukawa and McDougal [22] can be determined as

$$K_p = 1.643\times10^{-7}\left(\frac{d_{50}}{d_0}\right)^{1.57}\frac{{n_w}^3}{(1-n_w)^2},\quad d_0 = 10mm \tag{5}$$

where d_{50} is the mean stone size of the porous structure. The coefficient C_f can be approximate by

$$C_f = 100\left[d_{50}\left(\frac{n_w}{K_p}\right)^{1/2}\right]^{-1.5} \quad (6)$$

The inertial coefficient, S, accounts for the added mass effect and is widely taken as unity as this effect is usually negligible in comparison with other resistance terms [3,12,23]. It should be noted that although Eq. (4) has been widely adopted and validated by coastal engineering researchers [15,24], many other practical models of resistance forces are available and a thorough review on the subject can be found in Losada et al.[24] and Ren et al. [15].

2.3 Interface conditions

Since the domains inside and outside the porous media are governed by two separate sets of equations, it is necessary to provide appropriate interface conditions. For the kinematic condition, the continuity of Darcy velocity is adopted [4,7] to form

$$\boldsymbol{u}_l = n_w \boldsymbol{u}_p \quad (7)$$

Strictly the free flow just outside the porous media is not equivalent to the spatially averaged flow just inside the porous media because the flow contains numerous jets and wakes. The adoption of this simple condition is justified on the ground that the practical concern of wave over the porous structure is mainly on wave transmission, reflection and energy dissipation caused by porous media, which are not significantly affected by this assumption of mean velocity equivalence at the interface [4].

As for the dynamic conditions, they include the continuity of normal stress

$$p_l - \tau_{l,n} = p_p - \tau_{p,n} \quad (8)$$

and tangential stress

$$\tau_{l,\tau} = \tau_{p,\tau} \quad (9)$$

where $\tau_{l,n}$ and $\tau_{l,n}$ are normal viscous stresses on either side of the interface, $\tau_{l,\tau}$ and $\tau_{p,\tau}$ are tangential viscous stresses, which can be expressed by

$$\tau_{i,n} = 2\mu n_j\left(\frac{\partial u_j}{\partial n}\right)$$

$$\tau_{i,\tau} = \mu\left[n_j\left(\frac{\partial u_j}{\partial \tau}\right) + \tau_j\left(\frac{\partial u_j}{\partial n}\right)\right] \quad j = 1,2$$

with $\boldsymbol{n} = (n_1, n_2)$ and $\boldsymbol{\tau} = (\tau_1, \tau_2)$ are the unit normal and tangent vectors respectively to the interface. This work proposes a new numerical scheme imposing both types of conditions on a sharp interface and maintaining flow characteristics within each region.

2.4 Boundary conditions

Two types of boundaries are considered in this work, one of which is free surface condition by assigning zero pressure as

$$p_l = 0 \quad (10)$$

which is applied on the surface of the free flow only as the porous media is submerged.

On solid boundaries, walls either covered by porous structure or pure water, the slip condition is imposed as

$$\boldsymbol{u}_i \cdot \boldsymbol{n} = \boldsymbol{U} \cdot \boldsymbol{n} \qquad i = l,\ p \tag{11}$$

where $\boldsymbol{u}_i$ is the flow velocity either in porous media or outside it, $\boldsymbol{U}$ is the moving velocity of the boundary which can be zero representing a fixed wall or non-zeros as a wave generator. By applying Eq. (11) to the momentum equation, the pressure on solid boundary is governed by

$$\boldsymbol{n} \cdot \frac{\nabla p_i}{\rho} = \boldsymbol{n} \cdot \left(\boldsymbol{g} - \dot{\boldsymbol{U}} + \upsilon \nabla^2 \boldsymbol{u}_i + \mathbf{F}_i \right) \tag{12}$$

where $\dot{\boldsymbol{U}}$ the acceleration of the solid boundary that can be specified according to the wave generator used for each test case and F_i is the resistant force from porous structure which vanishes in the free flow domain, i.e. $F_l = 0$.

3. Numerical method

As shown in Figure 1, the entire simulation domain is split into two regions including a free flow region Q_l filled by hollow dots whose trajectories are governed by Eq. (2) and a porous flow region Q_p filled by solid dots governed by Eq. (4). Particles in region Q_l and Q_p, except the boundary particles, are known as inner particles. Their equation discretisation and particle moving update are based on MLPG_R method which is presented in Section 3.1. The interface Q_I is represented by a single layer of particles of shaded dots on which interface conditions are implemented by a new scheme as described in Section 3.2. The flow equations are solved separately in each region with physical characteristics (e.g. porosity and resistant forces) carried by individual particle and maintained within the region. It should be noted that most inner particles possess a complete support domain for particle approximation while for inner particles close to the interface (e.g. J_l in Figure 1), the support domain might be truncated with neighbouring particles only from its own region or the interface. For simultaneous coupling of two regions, interface particles in the new scheme have complete support domains including neighbouring particles from both regions.

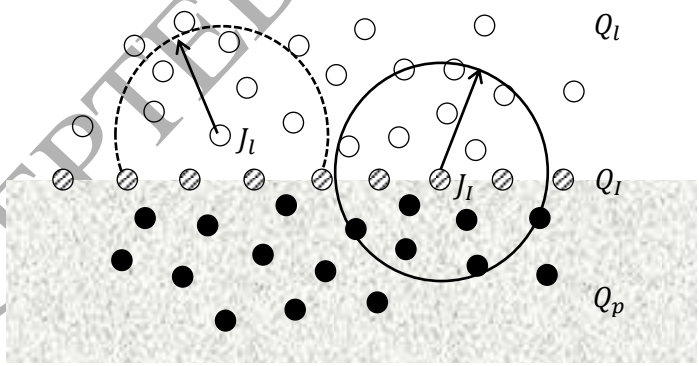

Figure 1: Computational domains consisting of three types of particles: particles in free flow domain of Q_l (hollow dots), in porous flow domain of Q_I (solid dots) and on the interface of Q_p (shaded dots). Particle $J_l \in Q_l$ has a support domain bounded by the dash circle which is the same case for particles in the porous region. The interface particle $J_I \in Q_I$ has a support domain bounded by the solid circle.

The governing equations are discretised and solved by the particle-based method in which the flow characteristics (e.g. $\boldsymbol{u}$, p etc.) will be stored on moving particles. When moving across the interface the particles will then be controlled by the corresponding governing equations and take up local properties including porosity and support domain. Since the model is for rigid porous structure, the

domain of porous region as well as the profile of the interface are prescribed and maintain throughout the simulation which are used for identifying to which domain particles belong. Within each flow domain and at each time step, pressure and velocity fields are solved using the prediction-correction scheme [25] with intermediate velocity predicted explicitly considering all the terms at RHS of the momentum equation except the pressure term as

$$\boldsymbol{u}_i{}^* = \boldsymbol{u}_i{}^n + \boldsymbol{g}\Delta t + \nu\nabla^2\boldsymbol{u}_i\Delta t + F_i\Delta t \qquad i = l,\ p \tag{13}$$

where n indicates the number of time step at which all the quantities are known to march to the next step. In Eq. (13), the subscript of i represents simulation domains, i.e. $i = l$ indicates the domain outside the porous media where extra resistant force $F_l = 0$ and $i = p$ is for the domain inside the porous media where $F_p = -\frac{\nu n_w}{K_p}\boldsymbol{u}_p - \frac{C_f {n_w}^2}{\sqrt{K_p}}\boldsymbol{u}_p|\boldsymbol{u}_p|$ as in Eq. (4). Then the pressure is updated in correction step by solving Pressure Poisson's Equation (PPE) expressed as

$$\nabla^2 p_i{}^{n+1} = \frac{\rho}{\Delta t}\nabla\cdot\boldsymbol{u}_i{}^* \tag{14}$$

The particle velocity and position at t^{n+1} are then updated by

$$\boldsymbol{u}_i{}^{n+1} = \boldsymbol{u}_i{}^* - \frac{1}{\rho}\nabla p_i{}^{n+1}\Delta t \tag{15}$$

$$\boldsymbol{r}_i{}^{n+1} = \boldsymbol{r}_i{}^n + \boldsymbol{u}_i{}^{n+1}\Delta t \tag{16}$$

3.1 Inner particles

For inner particles, the PPE, i.e. Eq. (14), is solved by MLPG_R method where the discretisation is based on a weak form. The PPE is multiplied by a specific test function as proposed in [25] and then integrated over a local sub-domain to achieve the final formulation of Eq. (17)

$$\left(\int_{\partial\Omega_I}\frac{\boldsymbol{n}\cdot(p_i\nabla\varphi)}{\rho_i}dS - \frac{p_i}{\rho_i}\right) = \int_{\Omega_I}\frac{\boldsymbol{u}_i{}^*\cdot\nabla\varphi}{dt}d\Omega \qquad i = l,p \tag{17}$$

where $\boldsymbol{n}$ is the unit vector normal to integration sub-domain Ω_I and pointing outside, $\varphi = \frac{1}{2\pi}ln(r/R_I)$ is the test function employing the solution of the Rankine source in an unbounded 2D domain with r being the distance away from the centre of the sub-domain. To discretize Eq. (17) moving least square (MLS) method is adopted for unknown pressure interpolation and a semi-analytical technique [25] is applied for numerical integration of the RHS of Eq. (17). The readers are referred to [25] for more derivation details. Other than directly discretizing the Eq. (17) by approximating second order derivatives of the unknown pressure in MPS [26] and ISPH [27] methods, this weak formulation only involves the approximation of pressure function itself. This feature potentially improves the accuracy in solving pressure equation and detailed comparisons and discussions are presented in [28].

3.2 Interface particles

In the following derivations, interface conditions, i.e. Eqs. (7) - (9) will be explicitly implemented on interface particles without introducing smoothing of any kind.

To implement stress and velocity conditions on the interface, the momentum equation for flow inside the porous media, i.e. Eq. (4), is first multiplied by the porosity n_w and then rearranged together with the momentum equation for the flow outside the media to obtain the expressions for pressure gradients as

$$\frac{\nabla p_l}{\rho} = -\frac{d\boldsymbol{u}_l}{dt} + \boldsymbol{g} + \upsilon\nabla^2\boldsymbol{u}_l \tag{18}$$

$$n_w\frac{\nabla p_p}{\rho} = -n_w\frac{d\boldsymbol{u}_p}{dt} + n_w\boldsymbol{g} + n_w\upsilon\nabla^2\boldsymbol{u}_p + n_w\boldsymbol{F}_p \tag{19}$$

Taking the first order Taylor series expansion of the pressure near the interface within each domain yields

$$\frac{1}{\rho}\left[p_l(\boldsymbol{r}_l) - p_l(\boldsymbol{r}_0)\right] = \frac{1}{\rho}\left(\nabla p_l\right)_{\boldsymbol{r}_0}\cdot\boldsymbol{r}_{l0} \tag{20}$$

$$\frac{n_w}{\rho}\left[p_p(\boldsymbol{r}_p) - p_p(\boldsymbol{r}_0)\right] = \frac{n_w}{\rho}\left(\nabla p_p\right)_{\boldsymbol{r}_0}\cdot\boldsymbol{r}_{p0} \tag{21}$$

where $\boldsymbol{r}_{l0} = \boldsymbol{r}_l - \boldsymbol{r}_0$, $p_l(\boldsymbol{r}_l)$ and $p_p(\boldsymbol{r}_p)$ are pressures outside and inside the porous media respectively at arbitrary point of $\boldsymbol{r}$ while $p_l(\boldsymbol{r}_0)$ and $p_p(\boldsymbol{r}_0)$ are the pressures obtained when $\boldsymbol{r}$ approaching points $\boldsymbol{r}_0$ from either sides of the interface, respectively with $\boldsymbol{r}_0$ being the position of the interface vector.

By discretising Eqs. (18) and (19) within the support domain outside and inside the porous media and replacing the pressure gradient term by Eqs. (20) and (21) respectively, it yields

$$\begin{aligned}&\frac{1}{\rho}\textstyle\sum_{k=1}^{n}\left[p_l(\boldsymbol{r}_k) - p_l(\boldsymbol{r}_0)\right]\phi(\boldsymbol{r}_{k0})\\ &\qquad = \textstyle\sum_{k=1}^{n}\left(-\frac{d\boldsymbol{u}_l}{dt} + \boldsymbol{g} + \upsilon\nabla^2\boldsymbol{u}_l\right)_{\boldsymbol{r}_0}\cdot\boldsymbol{r}_{k0}\phi(|\boldsymbol{r}_{k0}|)\end{aligned} \tag{22}$$

$$\begin{aligned}&\frac{n_w}{\rho}\textstyle\sum_{q=1}^{m}\left[p_p(\boldsymbol{r}_q) - p_p(\boldsymbol{r}_0)\right]\phi(\boldsymbol{r}_{q0})\\ &\qquad = \textstyle\sum_{q=1}^{m}\left(-n_w\frac{d\boldsymbol{u}_p}{dt} + n_w\boldsymbol{g} + n_w\upsilon\nabla^2\boldsymbol{u}_p + n_w\mathrm{F}_p\right)_{\boldsymbol{r}_0}\cdot\boldsymbol{r}_{q0}\phi(|\boldsymbol{r}_{q0}|)\end{aligned} \tag{23}$$

where the shape function $\phi(|\boldsymbol{r}|)$ is obtained by the moving least square (MLS) algorithm [20] with the weight function having no singularity and the support domain across the interface; $\boldsymbol{r}_k$ and $\boldsymbol{r}_q$ are position vectors of neighbouring particles outside and inside the porous media; n and m are total numbers of neighbouring particles in the two domains.

Adding up Eqs. (22) and (23) gives

$$\begin{aligned}&\frac{1}{\rho}\left[\sum_{k=1}^{n}p_l(\boldsymbol{r}_k)\phi(|\boldsymbol{r}_{k0}|) + n_w\sum_{q=1}^{m}p_p(\boldsymbol{r}_q)\phi(|\boldsymbol{r}_{q0}|)\right]\\ &\quad -\frac{1}{\rho}\left[p_l(\boldsymbol{r}_0)\sum_{j=1}^{n}\phi(\boldsymbol{r}_{l0}) - n_w p_p(\boldsymbol{r}_0)\sum_{j=1}^{n}\phi(\boldsymbol{r}_{p0})\right]\\ &\quad = \sum_{k=1}^{n}\left(-\frac{d\boldsymbol{u}_l}{dt}\right)_{\boldsymbol{r}_0}\cdot\boldsymbol{r}_{k0}\phi(|\boldsymbol{r}_{k0}|) + \sum_{q=1}^{m}\left(-n_w\frac{d\boldsymbol{u}_p}{dt}\right)_{\boldsymbol{r}_0}\cdot\boldsymbol{r}_{q0}\phi(|\boldsymbol{r}_{q0}|)\\ &\quad + \sum_{k=1}^{n}\left(g + \upsilon\nabla^2\boldsymbol{u}_w\right)_{\boldsymbol{r}_0}\cdot\boldsymbol{r}_{k0}\phi(|\boldsymbol{r}_{k0}|)\\ &\quad + \sum_{q=1}^{m}\left(n_w g + n_w\upsilon\nabla^2\boldsymbol{u}_p + n_w\mathrm{F}_p\right)_{\boldsymbol{r}_0}\cdot\boldsymbol{r}_{q0}\phi(|\boldsymbol{r}_{q0}|)\end{aligned} \tag{24}$$

From the velocity condition of Eq. (7), it can be deduced that $\frac{d\boldsymbol{u}_l}{dt} = n_w \frac{d\boldsymbol{u}_p}{dt}$ and the first two terms on the right hand side of Eq. (24) can be cancelled out by assuming that there exist sufficient neighbour particles surrounding the interface particle. However, to consider general particle distributions, two terms will be retained and is abbreviated as G_r with the particle acceleration from the last time step.

The normal stress condition of Eq. (8) is then substituted into Eq. (24) with the shear stress in normal direction calculated explicitly. Finally, two explicit expressions of pressures with a difference of $\tau_{l,n} - \tau_{p,n}$ for a single interface particle can be derived and the one on the porous side is

$$
\begin{aligned}
p_p(\boldsymbol{r}_0) = \frac{1}{\sum_{k=1}^{n}\phi(|\boldsymbol{r}_{k0}|) + n_w\sum_{q=1}^{m}\phi(|\boldsymbol{r}_{q0}|)}\Bigg[&\sum_{k=1}^{n} p_l(\boldsymbol{r}_k)\phi(|\boldsymbol{r}_{k0}|) \\
&+ n_w\sum_{q=1}^{m} p_p(\boldsymbol{r}_q)\phi(|\boldsymbol{r}_{q0}|) - \rho\sum_{k=1}^{n}(g + \upsilon\nabla^2\boldsymbol{u}_l)\cdot\boldsymbol{r}_{k0}\phi(|\boldsymbol{r}_{k0}|) \\
&- \rho\sum_{q=1}^{m}\left(n_w\boldsymbol{g} + n_w\upsilon\nabla^2\boldsymbol{u}_p + n_w\mathbf{F}_p\right)\cdot\boldsymbol{r}_{p0}\phi(|\boldsymbol{r}_{p0}|) - G_r \\
&- (\tau_{l,n} - \tau_{p,n})\sum_{k=1}^{n}\phi(|\boldsymbol{r}_{w0}|)\Bigg]
\end{aligned}
\qquad (25)
$$

where parameters at right hand side terms are from last time step. The pressure continuity condition which is a simplification of stress continuity is widely used in water wave simulations [4,15] based on the assumption that the shear stress difference in normal direction is negligible. This assumption can be applied to Eq. (25) by removing the last term at the right hand side resulting in a single pressure value at the interface particle. In the following tests, Eq. (25) is maintained with the other pressure value stored in the same particle for velocity update in two domains.

By enforcing velocity and normal stress conditions, the pressure is explicitly provided for interface particles as Dirichlet boundary for both domains. Meanwhile, following Shao [5] the tangential shear stress condition is implemented in velocity prediction step for intermediate velocity update. The present work is the first attempt to implement both dynamic and kinematic conditions in solving PPE stage through merging the two types of conditions to provide explicit pressure boundary value coupling the flow inside and outside the porous media. In this way, an efficient and physically sound model for flow over porous media is constructed by waiving extra numerical treatments. Since the interface consists of a single layer of fixed particles which can be regarded as having zero thickness, moving particles can be identified in either the pure fluid domain or porous domain and governed by the corresponding equations. When moving particles get very close to the interface or move across the interface from one domain to the other, their pressures are determined by the interface pressure expressed by Eq. (25). Although [11] adopted the same scheme, MLPG_R, to discretise the Poison's equation, the treatment of the interface follows [9, 10] involving the distribution of porosity smoothly over a layer of particles with the velocity near the interface being smoothed cross the layer to satisfy the velocity condition. Such treatment avoided the explicit condition implementation while extra computational cost was required for porosity and velocity interpolations. Since the thickness of the transitional layer is about twice the support domain, potential risk would also arise when the porous media becomes narrower.

3.3 Downstream wave absorbing boundary

To damp out unwanted wave reflection at the end of numerical tank, a damping zone is set up [29] by adding an artificial damping term in velocity updates as $\boldsymbol{u}_d{}^{n+1} = [1-\theta(x)]\boldsymbol{u}^{n+1}$ where $\boldsymbol{u}_d$ is damped velocity and the damping coefficient θ is defined as

$$\theta(x) = \frac{1}{2}\theta_0\left[1 - cos\left(\frac{\pi(x-x_d)}{L}\right)\right], \quad x > x_d$$

L is the length of damping zone taken as three times of wave length, x_d is the starting point of the damping zone and θ_0 is the magnitude of the maximum damping coefficient which is taken as 0.1.

3.4 Boundary particles

The zero-pressure boundary condition, i.e. Eq. (10), is applied on free surface particles which are identified at each time step based on particle number density and number of surrounding particles [20]. Other identification techniques such as divergence of a particle position [27] may also be used alternatively to track free surface especially in violent situations. The velocity and position update of free surface particle are based on Eqs. (15) and (16).

Implementing wall pressure condition of Eq. (12) effectively prevents particle penetration into rigid walls but requires discretisation of first order derivative of unknown pressure. In this work the gradient operator in MLPG_R method [30] with finite difference interpolation is adopted rather than MLS for the efficiency reason.

4. Model validation and application

In this section, the new interface boundary implementation method will be validated by analytical solutions of velocity and pressure along the interface and against experimental data of wave profiles and velocities at specific time instants and locations involving both solitary and propagating waves. Adaptive time step will be used following Courant condition as

$$\Delta t = C_r\,\Delta l_0/|\boldsymbol{u}|_{max}$$

where Δl_0 is initial particle distance, $|\boldsymbol{u}|_{max}$ is maximum velocity magnitude in the whole flow domain and C_r is Courant number taken as 0.1 [31] considering the probable reduced particle distance during simulations.

4.1 Solitary wave over porous bed

Amplitude attenuation of a solitary wave propagating over a porous bed has been a benchmark for numerical simulation as the rate of attenuation, wave profile and velocity at the interface are analytically available [32] for small-amplitude waves. The proposed model will be examined in all those aspects in the tests that the wave is initially generated by a piston type generator as shown in Figure 2. The depths of porous bed and pure fluid are $h_p = 0.4m$ and $h_0 = 0.4m$, respectively, $L = 25m$ is the length of tank filled by porous bed while $L_s = 2.5m$ is the length of wave generation zone on an impermeable bed aiming to provide a desired incident wave free from the influence of the porous bed. A small incident solitary wave with initial amplitude of $H_i = 0.06m$ is generated. The porous bed consists of granular material with mean diameter of $d_{50} = 5.5mm$ and porosity of $n_w = 0.39$. According to Eqs. (5) and (6), the intrinsic permeability and turbulent coefficient are determined to be $K_p = 0.102 \times 10^{-7}m^2$ and $C_f = 0.51$.

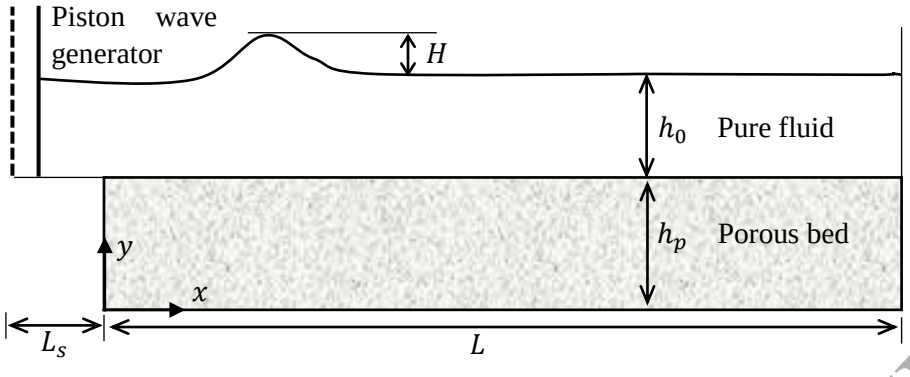

Figure 2: Numerical tank setup with coordinate system and notations.

The particle distance convergent tests are carried out first by using 15, 20 and 25 particles along the water depth corresponding to $\Delta l_0 = 0.027\text{m}, 0.020\text{m}$ and 0.016m respectively. Comparisons between numerical and analytical solutions [32] are shown in Figure 3 demonstrating that $\Delta l_0 = 0.02m$ is capable of giving a convergent result close to that of an even smaller distance of $\Delta l_0 = 0.016m$ and that the numerical results agree well with the analytical solution with an overall error of 0.53%. The analytical solution of the decay rate against the wave propagating distance is obtained from

$$\frac{H}{H_i} = \frac{1}{1+C_s(H_i/H_0)(x/H_0)} \qquad (26)$$

where $C_s = 0.4(K/C_0)\left(h_p/h_0\right)$, C_0 is wave speed expressed by $C_0 = \sqrt{gh_0}\left(1+\frac{H_i}{2h_0}\right)$, K is hydraulic conductivity can be linked to intrinsic permeability as $K = K_p g/\nu$ and x is the travelling distance on the porous bed.

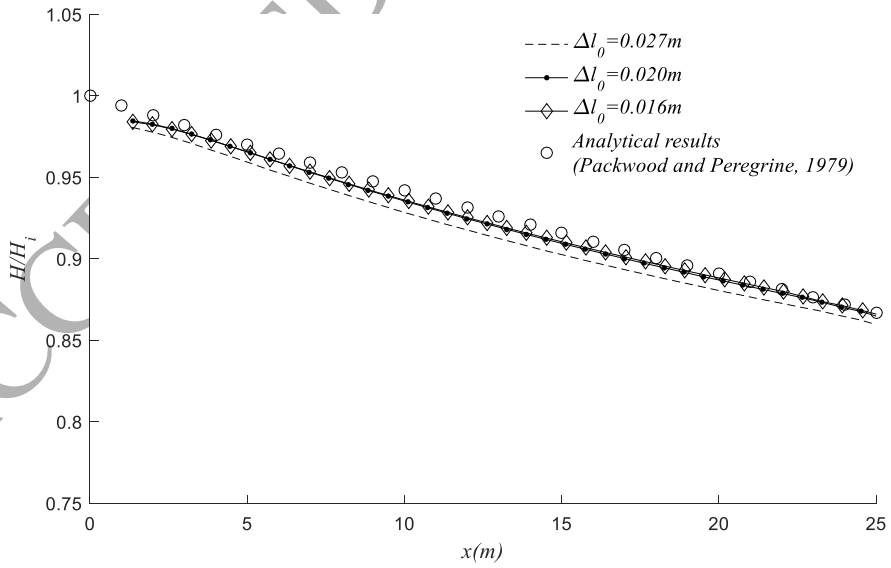

Figure 3: Comparison of amplitude attenuations calculated with particle distances of 0.027m (dash line), 0.02m (solid circle), 0.016m (diamond) and the analytical solution [32].

The wave surface profiles at three time instants, i.e. $t = 6.06\text{s}$, 9.09s and 12.12s, simulated with $\Delta l_0 = 0.02\text{m}$ are also examined against analytical solution with decayed amplitude and the profile expressed by

$$\eta = H(x)sech^2 b(x - C_0 t),\ b = \sqrt{3H(x)/4{h_0}^3} \quad (27)$$

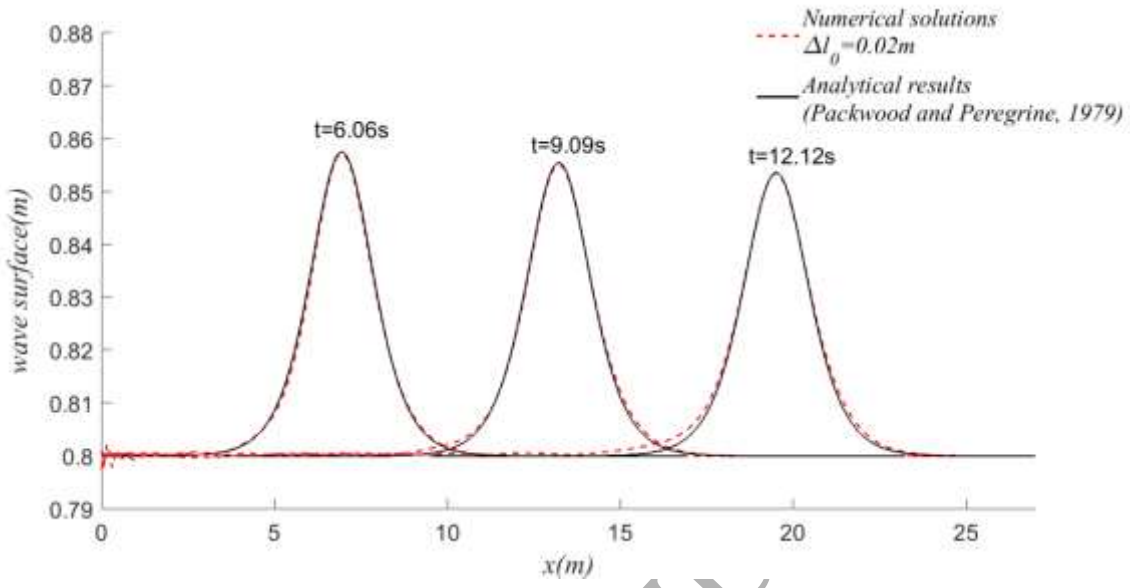

Figure 4: Comparison of analytical (black solid line) and simulated (red dash line) wave surfaces at three time instants of 6.06s, 9.09s and 12.12s.

As shown in Figure 4, the wave profile as well as the wave propagating speed are well captured by the model. To further test the accuracy of the interface conditions, comparisons are carried out for velocities at the interface. The analytical solutions of the velocities are

$$\frac{u(x)}{K} = \epsilon\sqrt{3\epsilon}\, sech^2 b(x - C_0 t) tanhb(x - C_0 t) \quad (28)$$

$$\frac{v(x)}{K} = \frac{3h_p\epsilon^2}{2h_0} sech^2 b(x - C_0 t)[2 - 3sech^2 b(x - C_0 t)] \quad (29)$$

where $\epsilon = H(x)/h_0$. The velocities given by Eqs. (28) and (29) and plotted in Figure 5 are Darcy velocities in the porous media which also match the velocity in the free flow domain. Figure 5 presents the horizontal and vertical velocities at $t = 6.06s$ when the wave crest reaches $x = 6.95m$. It should be noted that although the properties of the wave and porous bed in the simulation are set identical to that of the analytical solutions, some differences are expected as the analytical solutions are derived from the Darcy's law and the tangential velocity condition is neglected [32] while the numerical results are obtained from the full NS equations satisfying the continuity of both normal and tangential velocities. This difference is responsible for the slight discrepancies in velocity comparison, especially in the horizontal velocity.

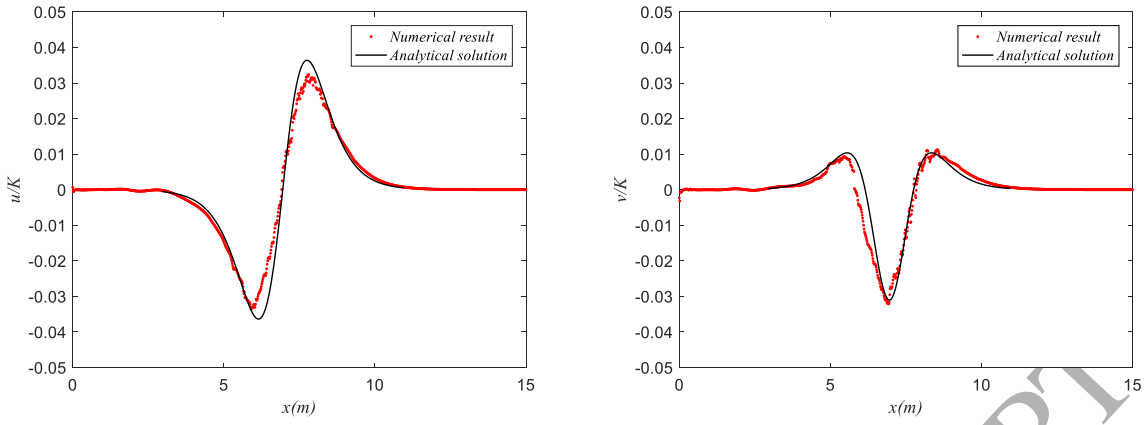

(a) (b)

Figure 5: Comparison of horizontal (a) and vertical (b) velocities on the interface between analytically solution (black lines) and numerical simulation with $\Delta l_0 = 0.02$m (red dots) at $t = 6.06s$.

4.2 Solitary wave interaction with porous breakwater

For validation of the model against experimental data, laboratory tests of solitary waves propagating over a porous breakwater [33] are selected. In this experiment, not only surface evolutions but also spatial velocity distributions are measured and can be used to verify the proposed interface treatment method.

Following the experimental setup, a numerical wave tank with length $L = 25m$ filled up with water to $h_0 = 0.106$m is initially generated as shown in Figure 6. At the left end of the tank a piston-type wave maker is equipped to generate the desired solitary wave and at the far opposite end there is a 5m long wave damper. A porous breakwater with depth of $h_1 = 6.5cm$ and width of $b = 13cm$ is located on the bottom of the tank and its intersection with the weather side of the breakwater is set to be the origin of the coordinate. The breakwater consists of uniform spheres with dimeter of d_{50} =1.5cm yielding a porosity of n_w =0.52. The wave amplitude examined at $x = -1.8m$ is taken as initial amplitude a =0.0477m at which point time also starts counting from $t = 0$.

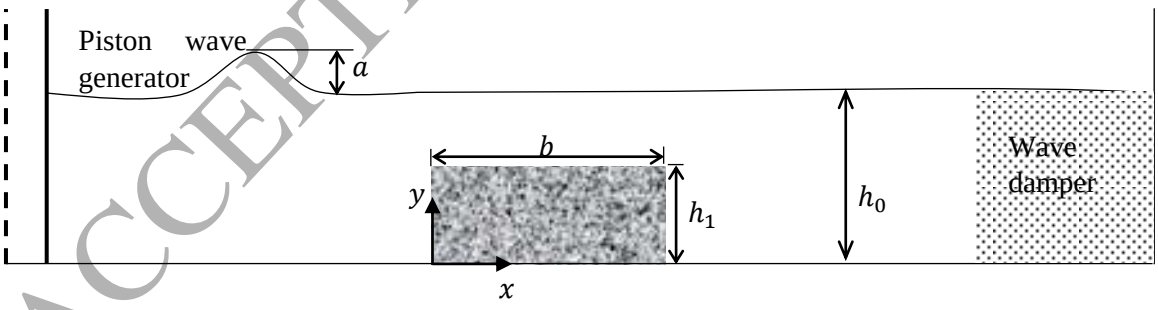

Figure 6: Numerical setup for solitary wave interacting with porous breakwater.

To verify the numerical convergence against particle distance, simulations with 30, 40 and 50 particles along the water depth corresponding to $\Delta l_0 = 3.5, 2.7$ and 2.1mm are carried out. Three sets of results are largely similar and agreed well with the experimental data. The velocity at x=0.16m along the water depth at t=1.65s is shown in Figure 7 indicating the convergence of the simulation. Results from [16] using ISPH method with smeared interface are also demonstrated in Figure 7 which show lower capability in capturing velocity variation along the depth comparing to the current model. The section examined is at the lee side of the breakwater where a vortex is formed when the wave passed over and velocities are sensitive to water depth. An overview of special and temporal flow

fields will be demonstrated in the following sections. As shown in Figure 7, results are well agreed with minor deviations from the experimental data which may be caused by numerical diffusion. Since $\Delta l_0 = 2.7mm$ is capable of obtaining almost the same result as that with even smaller distance, this particle distance will be adopted for the subsequent simulations of this case unless otherwise stated.

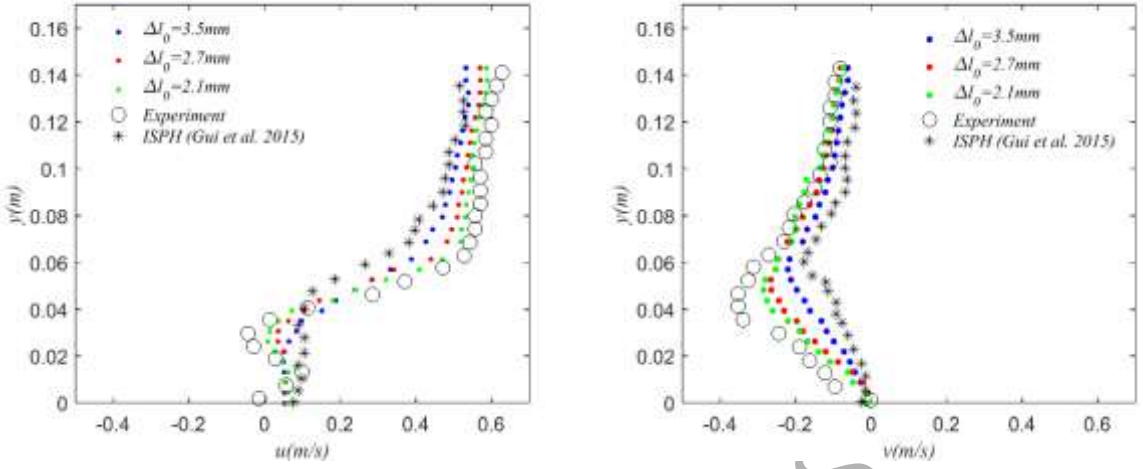

(a) (b)

Figure 7: Horizontal (a) and vertical (b) velocities through water depth at x=0.16 and t=1.65s, simulation results with initial particle distances of 3.5mm (blue), 2.7mm (red) and 2.1mm (green), experimental data (hollow circles) and results from ISPH method [16] (stars).

In Figure 8 to Figure 10, flow characteristics at three time instants, t=1.45s, 1.65s and 1.85s, including dynamic pressure field, velocity field and free surface in red dots are shown together with the measured free surface indicated by hollow circles. Comparison for seven sectional horizontal and vertical velocities from x=-0.04m to x=0.2m are also shown. To clearly present velocity fields with original particle locations, only one sixth particles are depicted for demonstration purpose in (b) of figures from 8 to 10. Particles are not as uniform as initial setup due to their movement with the wave. Fair agreements of free surface elevations at three snapshots showing the wave approaching, across and leaving the breakwater can be observed in (a) of each figure. In general, the dynamic pressure reaches maximum at the wave crest and gradually reduces towards two sides of the crest, which corresponds to high particle velocity under the wave crest. However due to the presence of the breakwater, flow separation starts at t=1.45s at the top of the weather side (Figure 8(b)) where low pressure arises (Figure 8(a)). Similar phenomena can also be observed in Figure 9 and Figure 10 when the wave goes over and leaves the breakwater, in which low pressure zone corresponding to a vortex develops at the top of the lee side and moves forward with the size expanded.

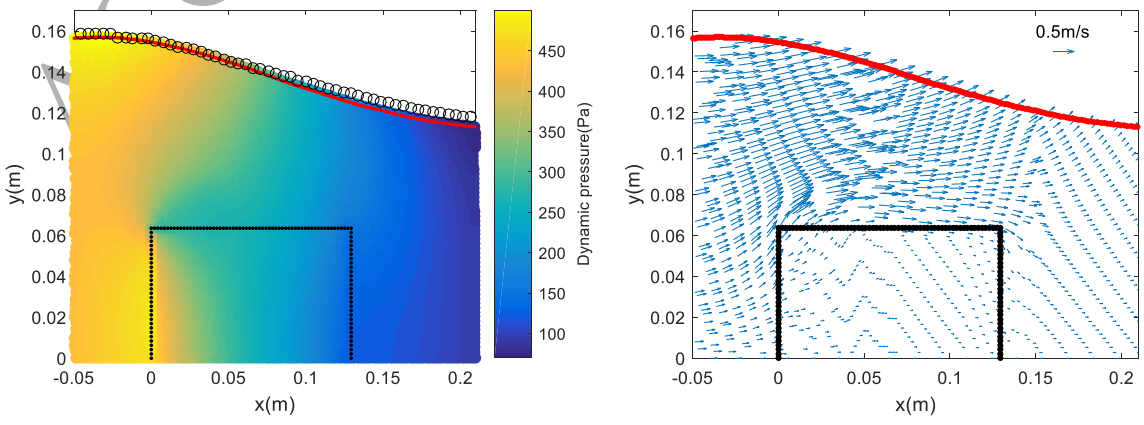

(a) (b)

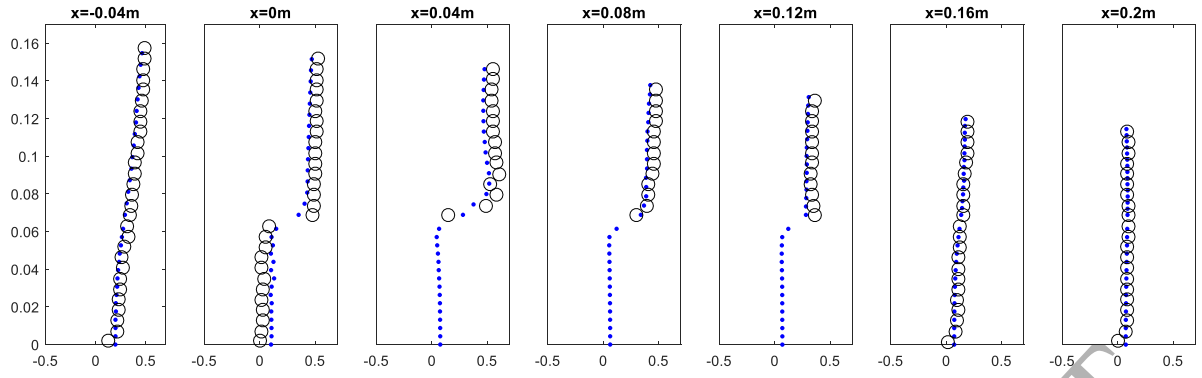

(c)

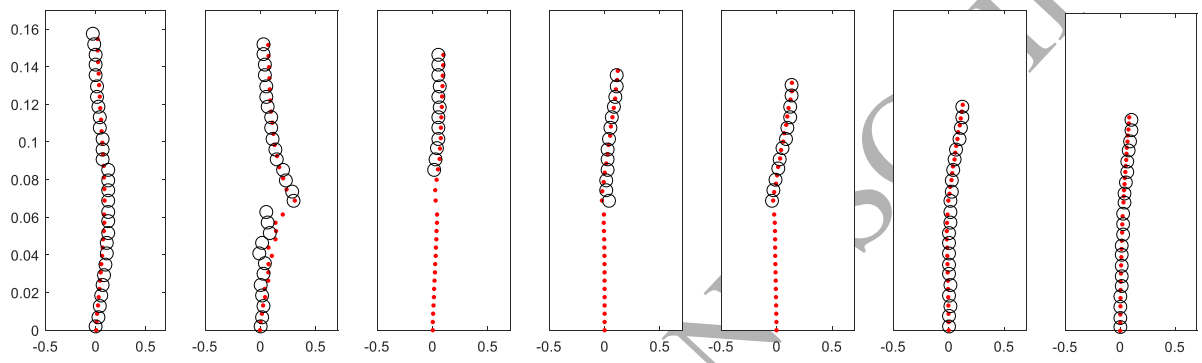

(d)

Figure 8: Simulated dynamic pressure and velocity fields at t=1.45s are shown in (a) and (b) with calculated free surface (red dot) compared with experimental data (black circle). Corresponding simulated (red dot) horizontal (c) and vertical (d) sectional velocities across the breakwater from -0.04m to 0.2m are compared with experimental data (black circle).

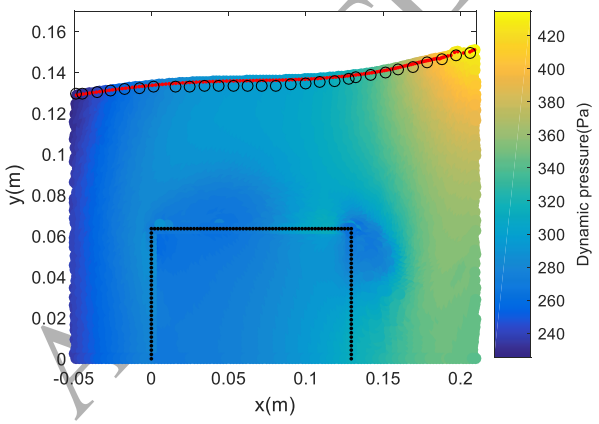

(a)

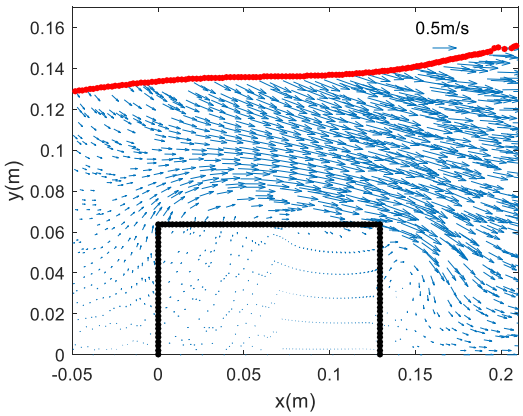

(b)

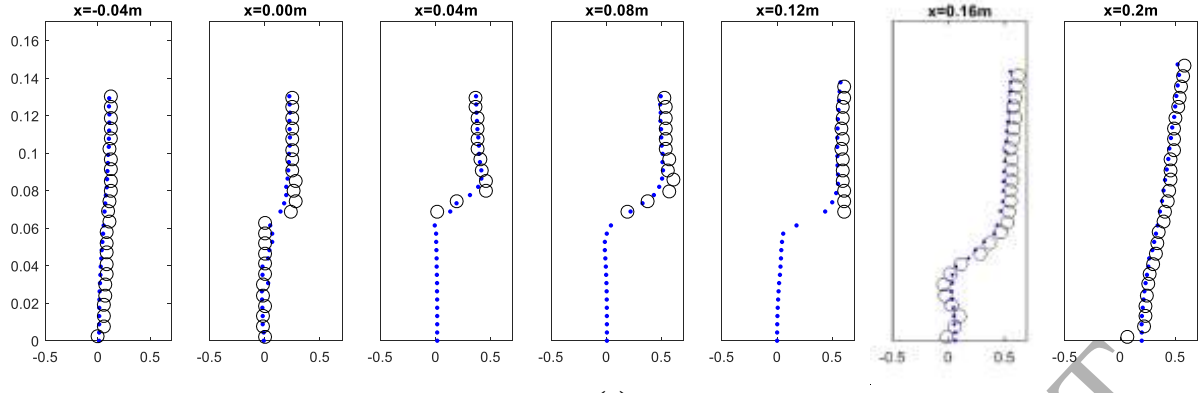

(c)

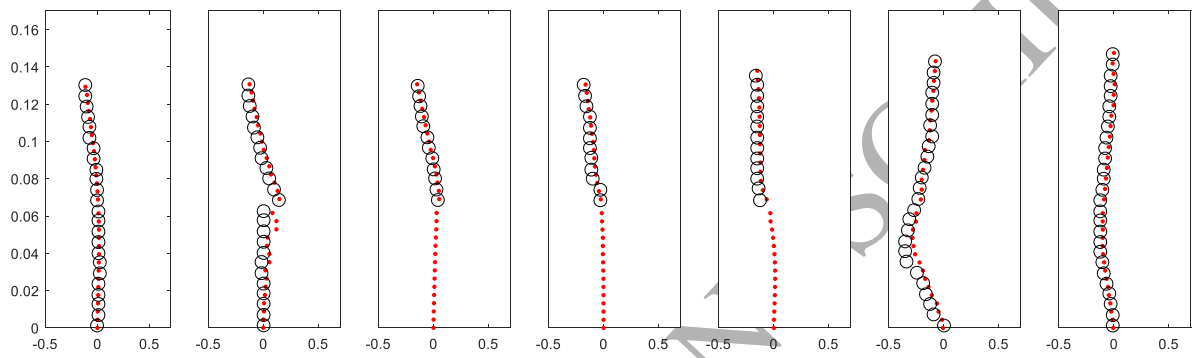

(d)

Figure 9: Simulated dynamic pressure and velocity fields at t=1.65s are shown in (a) and (b) with calculated free surface (red dot) compared with experimental data (black circle). Corresponding simulated (red dot) horizontal (c) and vertical (d) sectional velocities across the breakwater from -0.04m to 0.2m are compared with experimental data (black circle).

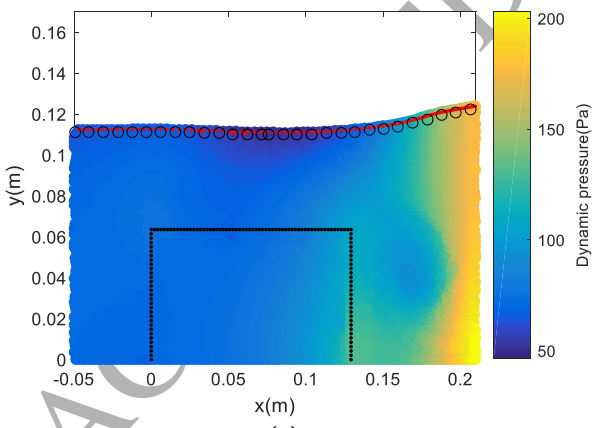

(a)

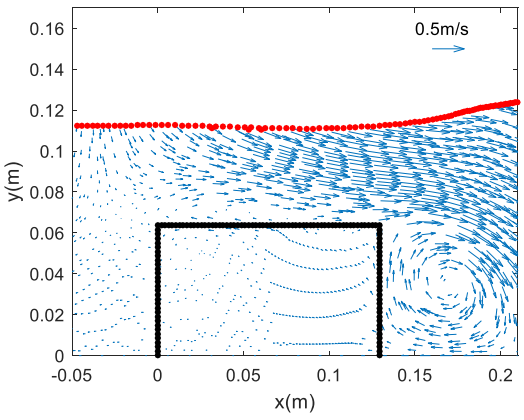

(b)

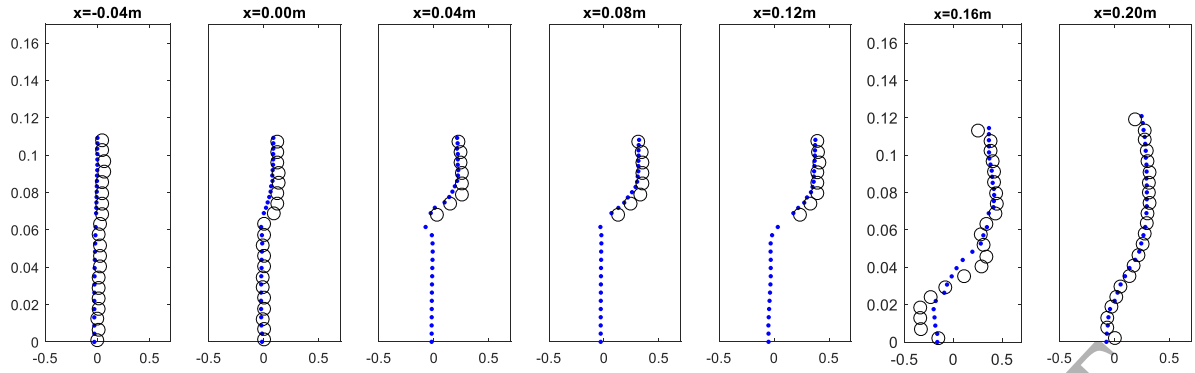

(c)

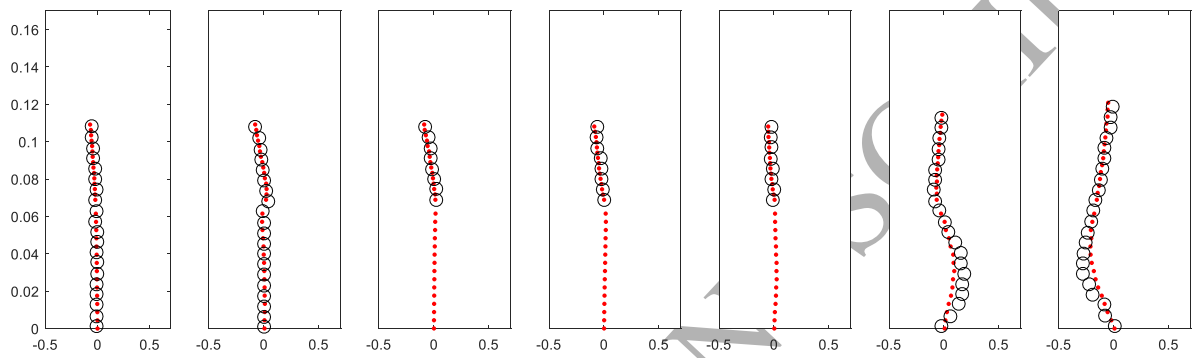

(d)

Figure 10: Simulated dynamic pressure and velocity fields at t=1.85s are shown in (a) and (b) with calculated free surface (red dot) compared with experimental data (black circle). Corresponding simulated (red dot) horizontal (c) and vertical (d) sectional velocities across the breakwater from -0.04m to 0.2m are compared with experimental data (black circle).

It can be seen from Figure 8 to Figure 10 that the sectional velocities for each time instant largely agree also with experimental data outside the porous zone. The discrepancies, generally underestimations, of velocities at the lee side of the breakwater when the wave passed are mainly caused by numerical diffusion introduced in estimating viscous term due to the large local velocity gradients.

4.3 Propagating wave over porous breakwater

To further test the performance of the new model on propagating wave interaction with porous media, the experiments of sinusoidal regular wave breaking on the porous breakwater [34] are simulated. Spatial variations of wave heights, surface elevation time histories for typical locations near the breakwater and field snapshots of pressure and velocity are examined in this case.

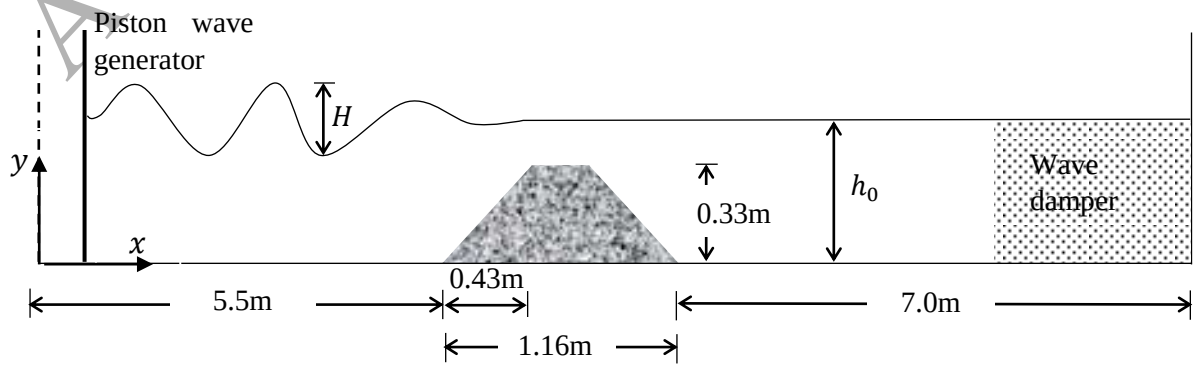

Figure 11: Numerical setup of the wave tank and the porous breakwater.

Following the experimental setup, a piston type wave generator and a wave damper 1.5L long where L is the wave length are located at two ends of the tank. A trapezoid breakwater with dimensions shown in Figure 11 is submerged in a water depth of $h_0 = 0.376$m. It is constructed by stones with mean diameter of $d_{50} = 25mm$ resulting in a porosity of 0.45. A sinusoidal wave is generated by the paddle movement of

$$s(t) = \frac{H_i}{2}(1 - cos\omega t)$$

where the initial wave height is $H_i = 0.092m$ and the frequency $\omega = 2\pi/T$ with the period set to be $T = 1.6s$. Since wave breaking on the breakwater is observed, the wave height distribution is monitored in the simulations using initial particle distances of 19mm, 13mm and 9mm by allocating 20, 30 and 40 particles along the water depth respectively. In Figure 12 it demonstrates that the convergence of the simulation almost achieves at $\Delta l_0 = 13mm$ as the results obtained are fairly close to that of using smaller particle distance, i.e. $\Delta l_0 = 9mm$. It can be seen that good agreement is achieved showing clear oscillations at the weather side due to wave reflection and wave breaking on the breakwater with the relative maximum height of 1.4. At the lee side, the height is reduced to a largely constant level around 0.8, damped by combined effects of porous resistance and wave breaking. Figure 13 illustrates the surface elevation variations against time at locations on the weather side (Figure 13 (a), (b) and (c)) and lee side (Figure 13 (d) and (e)). The weather side elevation variations are well captured by the model at both wave crest and trough while minor discrepancies can be observed at the lee side typically in the secondary wave formation although main variations have been largely captured. This may be caused by particle clustering at the water jet. Particle redistribution might be an effective way to address this issue which will be considered in the future work. Wave crest and trough on the breakwater are demonstrated in Figure 14 and Figure 15 together with dynamic pressure and velocity vectors. Smooth dynamic pressure variation can be observed across the domain including continuity at the interface even at the breaking point. The velocity reaches the maximum at the surface for both instants while the wave crest generates higher velocity than the trough. In this case, the porous breakwater is about to emerge from the water when wave trough interacts with it as shown in Figure 15. The model still works as there are a number of particles that can be identified as the free flow particles to determine the interface pressure in Eq. (25). As for the case that the breakwater is above the water surface, additional treatments for the free surface flow within the breakwater and for tracking the interface need to be carried out which is out of the scope of this work.

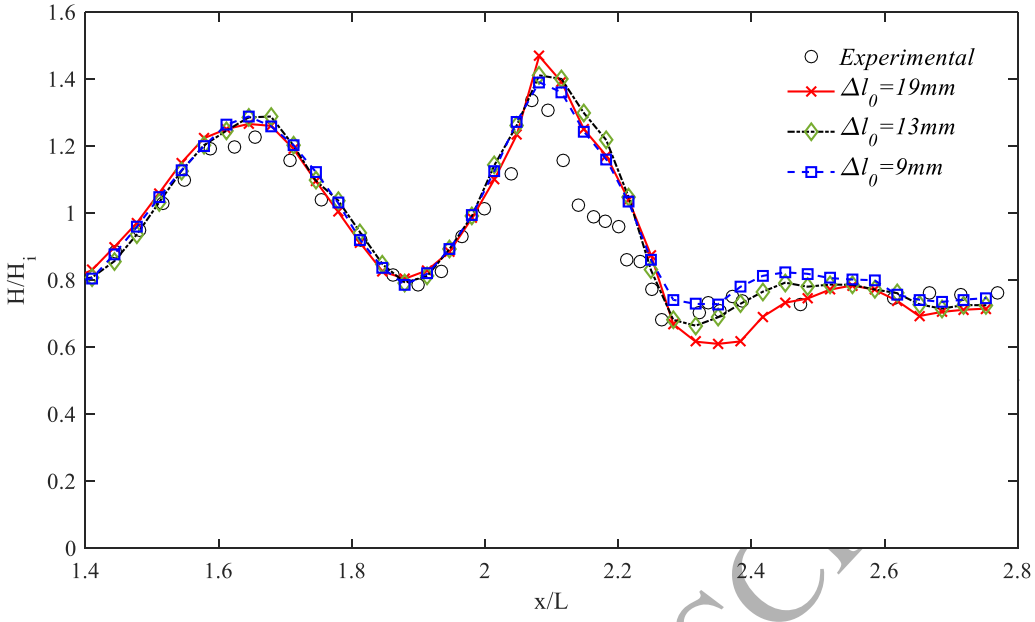

Figure 12: Wave height distributions, experimental data (hollow circle) and simulations with initial particle distances of 19*mm* (cross), 13*mm* (diamond) and 9*mm* (square).

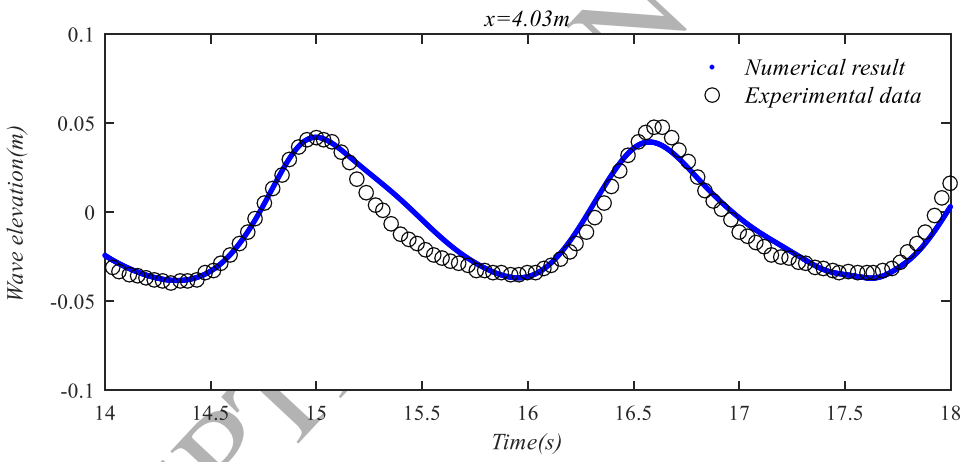

(a)

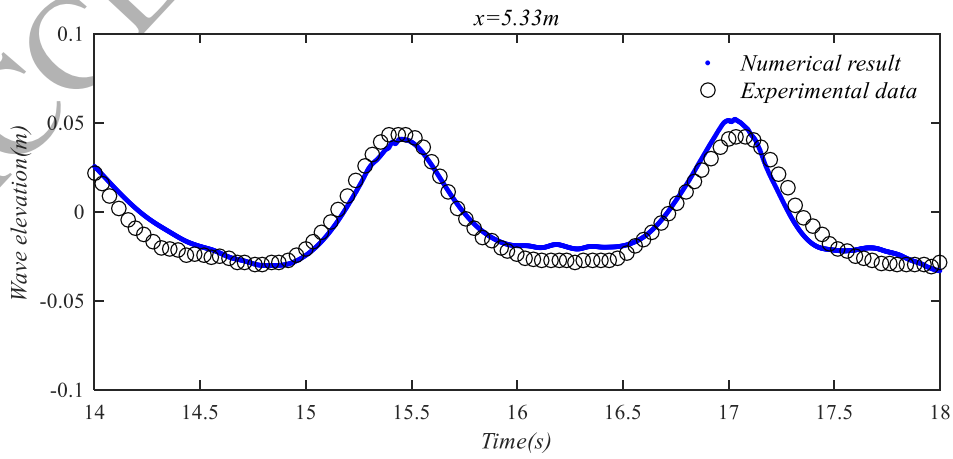

(b)

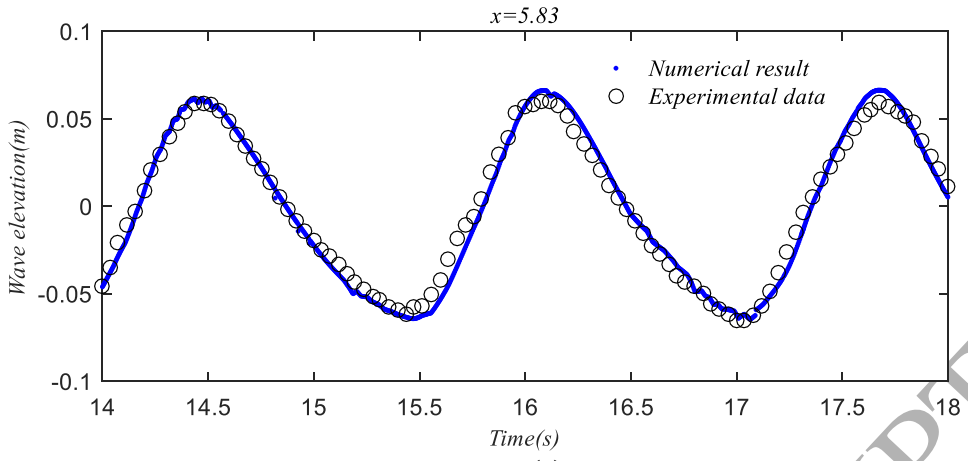

(c)

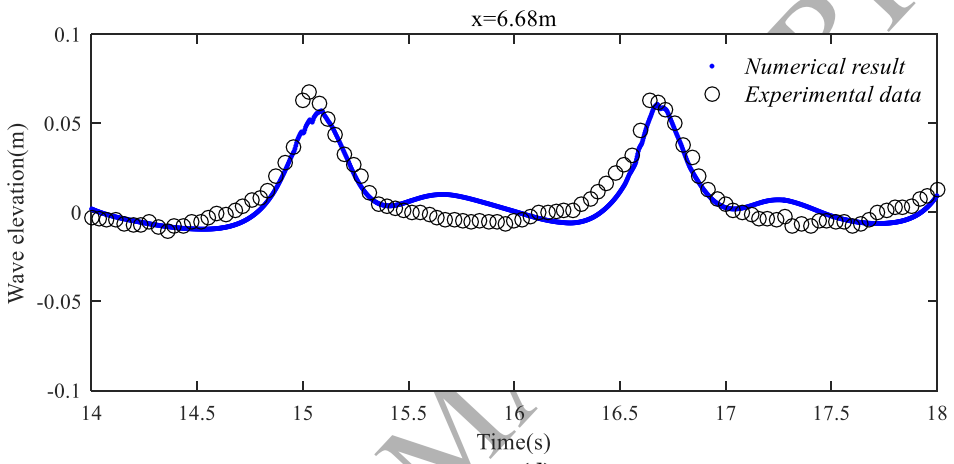

(d)

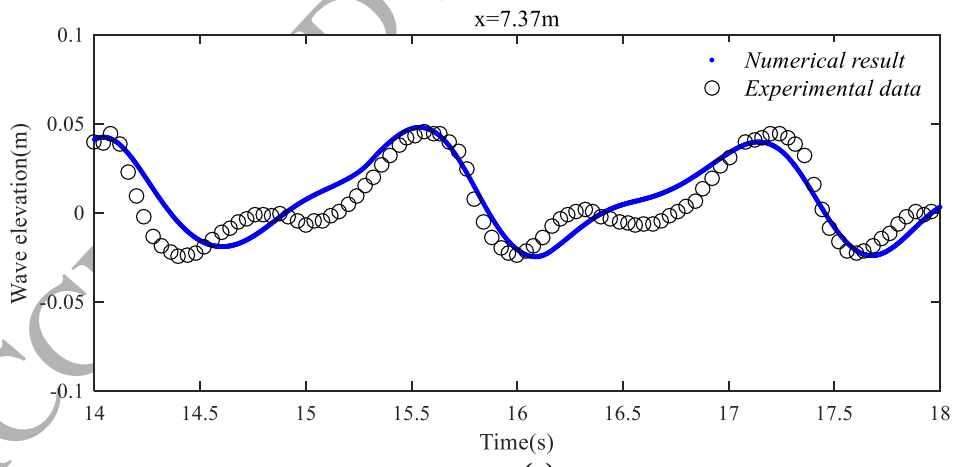

(e)

Figure 13: Comparisons of wave elevation time series at different locations between numerical results and experimental data.

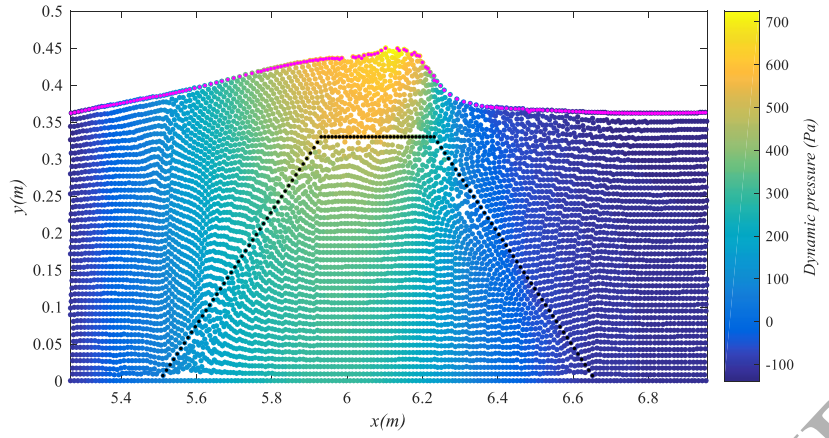

(a)

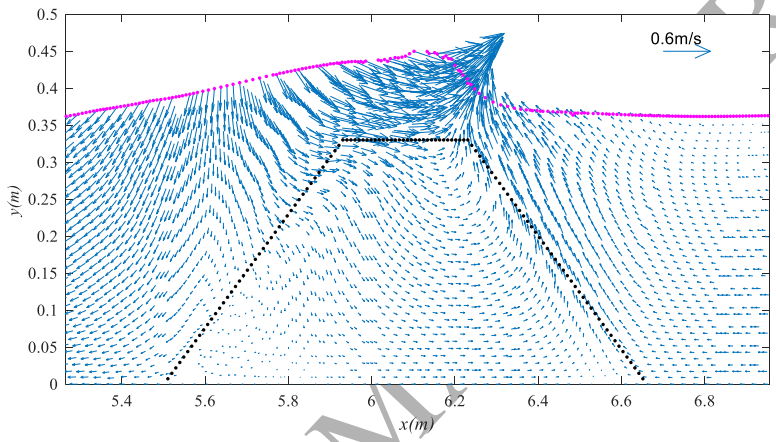

(b)

Figure 14: Snapshots of dynamic pressure (a) and velocity (b) under the wave crest on the breakwater. The free surface is plotted in purple.

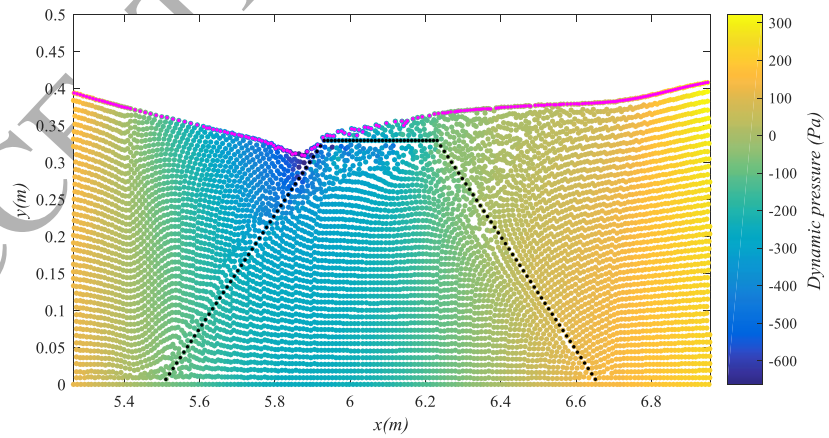

(a)

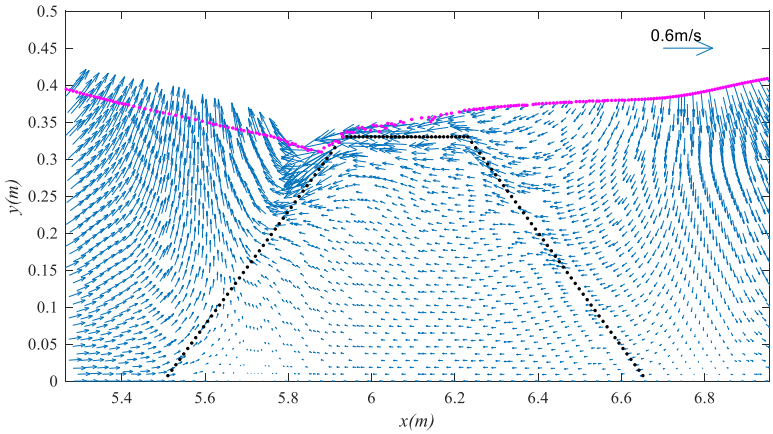

(b)

Figure 15: Snapshots of dynamic pressure (a) and velocity (b) of the wave trough on the breakwater. The free surface is plotted in purple.

5. Conclusion

The wave propagation in a porous/fluid domain is simulated using a particle method-based model by matching solutions of the Forchheimer equation in the porous region to the solution of NS equations at the interface between porous and fluid regions. The novel aspect of the work lies in the development of a new procedure to implement explicitly the interface boundary conditions on a single layer of fixed interface particles, thus dispensing the need for background nodes and artificial smoothing of porosity or other physical quantities. Resistant forces induced by granular materials are present only within the porous structure and drop abruptly to zero beyond the interface. The usual Darcy velocity and stress boundary conditions are recast in the form of explicit pressure expression so as to provide an effective Direchlet boundary for each flow domain. The interface conditions are implemented at PPE solving stage ensuring the accuracy of pressure field which is crucial in prediction-correction time marching procedure. The model is firstly validated by the analytical solutions of solitary wave over a porous bed with attenuation of wave height, wave profiles and velocities along the interface being well predicted. Further validations are carried out against experimental data involving propagating wave interaction with a porous breakwater. Good agreements are again achieved on wave surface elevations near the breakwater. Sectional velocities with the fields of dynamic pressure and velocity show a smooth transition across the interface as well as a clear flow separation at a low-pressure zone. The model is finally applied to the problem of wave breaking on a trapezoidal breakwater in which wave heights along the tank are examined and found to agree generally well with experimental data.

Acknowledgements

This work is partially supported by an EPSRC grant (EP/R02491X/1) through Newton Fund.

Reference

[1] I. J. Losada, R. A. Dalrymple, and M. A. Losada, "water waves on crown breakwaters," *J. Waterw. Port, Coastal, Ocean Eng.*, vol. 119, no. 4, pp. 367–380, 1993.

[2] C. K. Sollit and R. H. Cross, "Wave transmision through permeable break-waters," *Proc. 13th Coast. Eng. Conf.*, pp. 1827–1846, 1972.

[3] M. R. A. Van Gent, "Wave interaction with permeable coastal structures," *PhD Thesis, Delft Univ. Technol. Delft, Netherlands*, 1995.

[4] P. L. F. Liu, P. Lin, and T. Sakakiyama, "numerical modeling of wave interaction with porous structures," *J. Waterw. Port Coast. Ocean Eng.*, vol. 125, no. 6, p. 322, 1999.

[5] S. Shao, "Incompressible SPH flow model for wave interactions with porous media," *Coast. Eng.*, vol. 57, no. 3, pp. 304–316, 2010.

[6] P. H. Valvatne and M. J. Blunt, "Predictive pore-scale modeling of two-phase flow in mixed wet media," *Water Resour. Res.*, vol. 40, no. 7, pp. 1–21, 2004.

[7] M. R. A. Van Gent, "Porous flow through rubble-mound material," *J. Waterw. Port, Coast. Ocean Eng.*, vol. 121, no. 3, pp. 176–181, 1995.

[8] H. F. Burcharth and O. H. Andersen, "On The One Dimensional Steady And Unsteady Porous Flow Equations," *Coast. Eng.*, vol. 24, no. 94, pp. 233–257, 1995.

[9] H. Akbari and M. M. Namin, "Moving particle method for modeling wave interaction with porous structures," *Coast. Eng.*, vol. 74, pp. 59–7, 2013.

[10] B. Ren, H. Wen, P. Dong, and Y. Wang, "Numerical simulation of wave interaction with porous structures using an improved smoothed particle hydrodynamic method," *Coast. Eng.*, vol. 88, pp. 88–100, 2014.

[11] R. Divya and V. Sriram, "Wave-porous structure interaction modelling using Improved Meshless Local Petrov Galerkin method," *Appl. Ocean Res.*, vol. 67, pp. 291–305, 2017.

[12] C. J. Huang, M. L. Shen, and H. H. Chang, "Propagation of a solitary wave over rigid porous beds," *Ocean Eng.*, vol. 35, no. 11–12, pp. 1194–1202, 2008.

[13] M. F. Karim, K. Tanimoto, and P. D. Hieu, "Modelling and simulation of wave transformation in porous structures using VOF based two-phase flow model," *Appl. Math. Model.*, vol. 33, no.

1, pp. 343–360, 2009.

[14] P. Higuera, J. L. Lara, and I. J. Losada, “Three-dimensional interaction of waves and porous coastal structures using OpenFOAM. Part I: Formulation and validation,” *Coast. Eng.*, vol. 83, pp. 243–258, 2014.

[15] B. Ren, H. Wen, P. Dong, and Y. Wang, “Improved SPH simulation of wave motions and turbulent flows through porous media,” *Coast. Eng.*, vol. 107, pp. 14–27, 2016.

[16] Q. Gui, P. Dong, S. Shao, and Y. Chen, “Incompressible SPH simulation of wave interaction with porous structure,” *Ocean Eng.*, vol. 110, pp. 126–139, 2015.

[17] D. C. Conley and D. L. Inman, “Ventilated oscillatory boundary layers,” *J. Fluid Mech.*, vol. 273, no. C6, pp. 261–284, 1994.

[18] T. Sakakiyama and P. L. Liu, “Laboratory experiments for wave motions and turbulence f lows in front of a breakwater,” *Coast. Eng.*, vol. 44, pp. 117–139, 2002.

[19] Y. Zhou, “A sharp-interface treatment technique for two-phase flows in meshless methods,” *Comput. Fluids*, vol. 147, pp. 90–101, 2017.

[20] Q. W. Ma and J. T. Zhou, “MLPG_R Method for Numerical Simulation of 2D BreakingWaves,” *C. - Comput. Model. Eng. Sci.*, vol. 43, no. 3, pp. 277–303, 2009.

[21] R. A. Dalrymple and B. D. Rogers, “Numerical modeling of water waves with the SPH method,” *Coast. Eng.*, vol. 53, no. 2–3, pp. 141–147, 2006.

[22] K. Furukawa and W. G. McDougal, “Wave Diffraction Due to Trenches and Rubble,”, *Master Thesis, Oregon State University, US*, 1991.

[23] C. J. Huang, H. H. Chang, and H. H. Hwung, “Structural permeability effects on the interaction of a solitary wave and a submerged breakwater,” *Coast. Eng.*, vol. 49, no. 1–2, pp. 1–24, 2003.

[24] I. J. Losada, M. Asce, J. L. Lara, and M. Jesus, “Modeling the Interaction of Water Waves with Porous Coastal Structures,” *J. Waterw. Port, Coastal, Ocean Eng.*, vol. 142, no. 6, pp. 1–18, 2016.

[25] Q. W. Ma, “MLPG Method Based on Rankine Source Solution for Simulating Nonlinear Water Waves,” *C. - Comput. Model. Eng. Sci.*, vol. 9, no. 2, pp. 193–209, 2005.

[26] S. Koshizuka and Y. Oka, “Moving-particle semi-implicit method for fragmentation of incompressible fluid,” *Nuclear science and engineering*, vol. 123, no. 3. pp. 421–434, 1996.

[27] E. S. Lee, C. Moulinec, R. Xu, D. Violeau, D. Laurence, and P. Stansby, “Comparisons of weakly compressible and truly incompressible algorithms for the SPH mesh free particle method,” *J. Comput. Phys.*, vol. 227, no. 18, pp. 8417–8436, 2008.

[28] X. Zheng, Q. W. Ma, and W. Y. Duan, “Incompressible SPH method based on Rankine source solution for violent water wave simulation,” *J. Comput. Phys.*, vol. 276, pp. 291–314, 2014.

[29] Q. W. Ma, “Meshless local Petrov-Galerkin method for two-dimensional nonlinear water wave problems,” *J. Comput. Phys.*, vol. 205, no. 2, pp. 611–625, 2005.

[30] Q. W. Ma, “A New Meshless Interpolation Scheme for MLPG_R Method,” *C. - Comput. Model. Eng. Sci.*, vol. 23, no. 2, pp. 75–89, 2008.

[31] E. Y. M. Lo and S. Shao, “Simulation of near-shore solitary wave mechanics by an incompressible SPH method,” *Appl. Ocean Res.*, vol. 24, no. 5, pp. 275–286, 2002.

[32] A. R. Packwood and D. H. Peregrine, “The propagation of solitary waves and bores over a porous bed,” *Coast. Eng.*, vol. 3, pp. 221–242, 1979.

[33] Y. T. Wu and S. C. Hsiao, "Propagation of solitary waves over a submerged permeable breakwater," *Coast. Eng.*, vol. 81, pp. 1–18, 2013.

[34] P. D. Hieu and K. Tanimoto, "Verification of a VOF-based two-phase flow model for wave breaking and wave-structure interactions," *Ocean Eng.*, vol. 33, no. 11–12, pp. 1565–1588, 2006.